

Radiative electron capture to continuum in relativistic ion–atom collisions

D H Jakubaša-Amundsen

Physics Section, University of Munich, D-85748 Garching, Germany

Received 24 December 2002

Published

Online at stacks.iop.org/JPhysB/36/1

Abstract

The capture of a target electron to the projectile continuum with simultaneous photon emission, known as radiative ionization (RI), is investigated theoretically for fast, highly charged projectiles colliding with light target atoms. Based on the impulse approximation in its post form, the features of radiative ionization are studied and contrasted with the related processes of radiative electron capture and nonradiative electron capture to continuum (ECC). A large RI cusp asymmetry is found, increasing strongly with projectile charge but decreasing with projectile velocity. However, in contrast to ECC, the cusp is skewed to the high-energy side. Results are shown for 20 MeV amu⁻¹ Kr³⁶⁺ + H and for 100 and 400 MeV amu⁻¹ U⁹²⁺ on H and N.

1. Introduction

Radiative electron capture into bound states of heavy bare or one-electron ions has been a field of current interest ever since its discovery by Raisbeck and Yiou (1971), Schnopper *et al* (1972). Due to powerful accelerator facilities, radiative electron capture (REC) experiments were extended to the relativistic regime (Gould *et al* (1984), Anholt *et al* (1984); for recent research see, for example, Stöhlker *et al* (1995, 1997)). For uranium projectiles, REC into K, L and M shells could be identified (Stöhlker *et al* 1995, 1998). In addition, the photon spectra show a large low-energy background with a threshold-like behaviour at the series limit (Kienle *et al* 1973, Yamadera *et al* 1981, Ludziejewski *et al* 1998). This background has been interpreted in terms of radiative ionization (Jakubaša and Kleber 1975, Yamadera *et al* 1981) which can be viewed as continuation of REC across the ionization threshold of the projectile.

The interest in reinvestigating radiative ionization is twofold. First, a simultaneous measurement of the momentum of both emitted particles, electron and photon, is planned at the ESR storage ring of GSI in Darmstadt, Germany (Hagmann 2003). With this aim, the COLTRIMS detector technique, a 2D position-sensitive detector equipped with a forward electron spectrometer and a large solid-angle Ge x-ray detector, will be used. The analysis of the charge states of both projectile and recoil ion allows for a unique identification of the single ionization channel (Moshhammer *et al* 1994). When measured for bare projectiles in

[Processing](#)

[CRC data](#)

JPB/jpb157703-xsl/PAP	File name B	.TEX	First page
Printed 16/4/2003	Date req.		Last page
	Issue no.		Total pages
Focal Image	Artnum		Cover date
<i>(Ed.: STUART)</i>			

coincidence with bare ejectiles and singly ionized recoil ions at the radiative ionization (RI) cusp, one thus obtains an unambiguous experimental identification of the RI process.

Second, a comparison of the capture to continuum cusp shape from electron capture to continuum (ECC) and from RI provides a sensitive test of the influence of the additional photon degrees of freedom on the dynamics of target ionization. The ECC cusp has been studied extensively (for a review see Groeneveld *et al* 1984). It is strongly skewed to the low-energy side which can only be correctly described within a higher-order theory (Jakubaša-Amundsen 1983). While ECC is dominant at moderate collision velocities, the additional photon emission becomes important at very high velocities. The only comparison between ECC and RI existing so far (Martiarena and Garibotti 1985) is within the first-order Born theory for $p + \text{He}$ collisions and concerns only the absolute values.

RI is also closely related to bremsstrahlung emission of a fast electron in the field of the heavy projectile. In fact, within the impulse approximation (IA) the cross section for RI is basically obtained by folding the cross section for electron–nucleus bremsstrahlung with the momentum distribution of the electron in its initial state. The emitted photon carries away the excess energy of the electron, allowing for high capture-to-continuum cross sections even when the relative velocity between target and projectile is high.

Correspondingly, similar theoretical models are used for the description of these interrelated processes. Calculations on both radiative electron capture (Briggs and Dettmann 1974, Kleber and Jakubaša 1975) as well as radiative ionization (Jakubaša and Kleber 1975)¹ date back to the mid-1970s. Relativistic effects for REC were already considered by Spindler *et al* (1979) and Hino and Watanabe (1987) while a strict relativistic formulation of the theory was provided by Eichler (1990) and the first exact calculations (within the IA) were performed by Ichihara *et al* (1994). Electron–nucleus bremsstrahlung, the underlying process for RI, was already calculated by Elwert and Haug (1969), using semirelativistic Sommerfeld–Maue wavefunctions for the electron. A fully relativistic treatment was provided later (Tseng and Pratt 1971).

In the present work a relativistic formulation of the RI process is presented and the calculations are performed with Sommerfeld–Maue wavefunctions. This is a reasonable approximation according to Shaffer *et al* (1996) who have compared the exact bremsstrahlung theory with the Elwert–Haug results and with experiment for collision systems similar to those investigated here. The theory is formulated in section 2. Section 3 provides numerical results for the fourfold differential RI cross sections and RI cusp asymmetries in the case of projectiles up to U^{92+} at collision energies between 10 and 400 MeV amu^{-1} . Section 3 also gives a comparison between the cusp shapes of the RI and ECC processes. Conclusions are drawn in section 4. Atomic units ($\hbar = m = e = 1$) are used unless otherwise indicated.

2. Theory

We consider the case of an asymmetric collision and restrict ourselves to bare projectiles moving much faster than the target electrons according to their classical orbiting velocity. The target electrons are described within the independent particle model and the coupling to the photon field is treated to first order.

¹ In equation (1.2) of that paper, a factor $F = \frac{5}{2} + \frac{3}{4} \frac{2E - \hbar\omega}{E - \hbar\omega} \ln \frac{(\sqrt{E + \sqrt{E - \hbar\omega}})^2}{\hbar\omega}$ is missing. In equation (2.13), B should be replaced by 1, and correspondingly $G = B = 1$ in equation (2.20) in the case of the IA.

2.1. Transition amplitude

Target ionization into low-lying energy states with respect to the projectile frame of reference is described by means of electron capture to the continuum, i.e. the electron is emitted into a projectile eigenstate $\psi_{f,P}^{(\sigma_f)}$. Since we deal with light targets ($Z_P \gg Z_T$, where Z_P and Z_T are the nuclear charges of projectile and target, respectively), the electron–target interaction will be neglected not only in the final state, but also in the intermediate electronic states. The starting point is the general expression for the transition amplitude in its post form for ionization induced by the photon field \mathbb{A}' , which is given by

$$a_{fi} = -\frac{i}{c} \int d^4x' \overline{\psi_{f,P}^{(\sigma_f)'}}(x') d_\lambda^+ \mathbb{A}'(x') \hat{S} \Psi_i^{(\sigma_i)}(x) \quad (2.1)$$

where $\Psi_i^{(\sigma_i)}$ is the exact wavefunction relating asymptotically to the initial bound target state $\psi_{i,T}^{(\sigma_i)}$. σ_i and σ_f are the spin projections in the initial and final state, respectively. Primes denote quantities defined in the projectile frame of reference and $x' = (ct', \mathbf{x}')$ and $x = (ct, \mathbf{x})$ are the space and time coordinates of the electron in the projectile and target frame, respectively. Since we deal with a heavy projectile, the calculation is conveniently performed in the projectile's rest system. Therefore, $\Psi_i^{(\sigma_i)}$, defined in the target frame, has to be transformed by means of the Lorentz boost operator \hat{S} .

When the coupling is exclusively due to the photon field, one has

$$\gamma_0 \mathbb{A}'(x') = -\alpha \mathbf{A}'(x') \quad (2.2)$$

with γ_0 and α Dirac matrices (Rose 1971) and the photon field given by

$$\mathbf{A}'(x') = \mathbf{A}'_\lambda e^{ik'x'} d_\lambda^+, \quad \mathbf{A}'_\lambda = \sqrt{\frac{c^2}{(2\pi)^2 \omega'}} e_\lambda \quad (2.3)$$

where d_λ^+ is the creation operator of a photon with 4-momentum $k' = (\frac{\omega'}{c}, -\mathbf{k}')$ and polarization direction e_λ .

Describing the wavefunction $\Psi_i^{(\sigma_i)}(x)$ by means of the Lippmann–Schwinger equation (Bjorken and Drell 1964, p 107) and neglecting all interactions except the electron–projectile Coulomb field one gets

$$\hat{S} \Psi_i^{(\sigma_i)}(x) \equiv \Psi_i^{(\sigma_i)'}(x') = \int d^4y' \left[\delta(x' - y') + \frac{1}{c} S'_P(x', y') \mathbb{A}'_P(y') \right] \psi_{i,T}^{(\sigma_i)'}(y') \quad (2.4)$$

where \mathbb{A}'_P denotes the electron–projectile interaction and $S'_P(x', y')$ describes the electron propagation in this field. One can simplify (2.4) by using the definition of a projectile scattering eigenstate $\psi_{q,P}^{(s)'}(x')$ of momentum q and spin projection s' :

$$\int d^4y' \left[\delta(x' - y') + \frac{1}{c} S'_P(x', y') \mathbb{A}'_P(y') \right] q'_s(y') = \psi_{q,P}^{(s)'}(x') \quad (2.5)$$

where

$$q'_s(x') = \frac{1}{(2\pi)^2} u_q^{(s)} e^{iqx' - i\delta_s \omega_q t'} \quad (2.6)$$

$$u_q^{(s)} = \left(\frac{\omega_q + mc^2}{2\omega_q} \right)^{1/2} \left(1 + \delta_s \alpha \mathbf{q} \frac{c}{\omega_q + mc^2} \right) e_s, \quad s = 1, \dots, 4, \omega_q = \sqrt{q^2 c^2 + c^4}$$

is a relativistic plane wave (Rose 1971) of energy $\delta_s \omega_q$ with $\delta_s = +1$ for the particle states ($s = 1, 2$) and -1 for the antiparticle states ($s = 3, 4$), and e_s a 4D unit vector.

A complete set of plane waves (2.6) is introduced into (2.4) where the energy ω_q in the phase factor of q'_s is treated as an independent variable. However, an on-shell approximation

is made by keeping $\omega_q = \sqrt{q^2 c^2 + c^4}$ in the definition of the spinor $u_q^{(s)}$. This on-shell approximation is reasonable for light targets as it corresponds to neglecting the binding of the electron in its initial state. Then (2.4) turns into

$$\Psi_i^{(\sigma_i)'}(x') = \frac{1}{c} \sum_{s=1}^4 \int d\mathbf{q} d\omega_q \psi_{q,P}^{(s)'}(x')(q'_s(x'), \psi_{i,T}^{(\sigma_i)'}(x')) \quad (2.7)$$

where the brackets (\cdot, \cdot) denote integration over x' . When (2.7) is inserted into (2.1) and $\bar{\psi} = \psi^\dagger \gamma_0$ is used, one obtains the transition amplitude in the IA:

$$a_{fi}^{\text{IA}} = \frac{i}{c} A'_\lambda \int d^4 x' \psi_{f,P}^{(\sigma_f)'+}(x') \alpha \mathbf{e}^{ik'x'} \frac{1}{c} \sum_{s=1}^4 \int d\mathbf{q} d\omega_q \psi_{q,P}^{(s)'}(x')(q'_s(x'), \hat{S} \psi_{i,T}^{(\sigma_i)}(x)). \quad (2.8)$$

One thus obtains a factorization into two matrix elements. The first of them describes inelastic electron scattering from the radiation field. Splitting $d^4 x'$ into $c dt' d\mathbf{x}'$ and separating the time dependence, one gets

$$\int d^4 x' \psi_{f,P}^{(\sigma_f)'+}(x') \alpha \mathbf{e}^{ik'x'} \psi_{q,P}^{(s)'}(x') = \frac{c}{\sqrt{2\pi}} \mathbf{W}_{\text{rad}}(\sigma_f, s, q) 2\pi \delta(E'_f + \omega' - \delta_s \omega_q) \quad (2.9)$$

with

$$\mathbf{W}_{\text{rad}}(\sigma_f, s, q) = \int d\mathbf{x}' \psi_{f,P}^{(\sigma_f)'+}(\mathbf{x}') \alpha \mathbf{e}^{-ik'\mathbf{x}'} \psi_{q,P}^{(s)'}(\mathbf{x}') \quad (2.10)$$

and E'_f is the electronic final-state energy (including the rest mass).

For the evaluation of the second matrix element in (2.8) another complete set of free states, $p_\sigma(x)$, now defined in the target frame of reference, is introduced such that

$$M := \frac{1}{c} (q'_s(x'), \hat{S} \psi_{i,T}^{(\sigma_i)}(x)) = \frac{1}{c^2} \sum_{\sigma=1}^4 \int d\mathbf{p} d\omega_p (q'_s(x'), \hat{S} p_\sigma(x)) (p_\sigma(x), \psi_{i,T}^{(\sigma_i)}(x)). \quad (2.11)$$

The second term in brackets is readily expressed in terms of the initial-state wavefunction in momentum space: $\varphi_{i,T}^{(\sigma_i)}(\mathbf{p})$,

$$\begin{aligned} \frac{1}{c} (p_\sigma(x), \psi_{i,T}^{(\sigma_i)}(x)) &= \frac{1}{c} \int d\mathbf{x} c dt \frac{1}{(2\pi)^2} u_p^{(\sigma)+} e^{-ip\mathbf{x} + i\delta_\sigma \omega_p t} \psi_{i,T}^{(\sigma_i)}(\mathbf{x}) e^{-iE_i^T t} \\ &= \sqrt{2\pi} u_p^{(\sigma)+} \varphi_{i,T}^{(\sigma_i)}(\mathbf{p}) \delta(\delta_\sigma \omega_p - E_i^T) \end{aligned} \quad (2.12)$$

where E_i^T is the energy of the bound target electron and $\delta_\sigma = +1$ for $\sigma = 1, 2$ and -1 for $\sigma = 3, 4$. For the first term, the Lorentz boost operator \hat{S} and the transformation connecting x to x' have to be specified (Bjorken and Drell 1964, Jakubaša-Amundsen 1997):

$$\begin{aligned} \hat{S} &= \sqrt{\frac{1+\gamma}{2}} \left(1 - \frac{\gamma v/c}{1+\gamma} \alpha_z \right) \\ x &= \Gamma x' + b, \quad \Gamma = \begin{pmatrix} \gamma & 0 & 0 & \gamma v/c \\ 0 & 1 & 0 & 0 \\ 0 & 0 & 1 & 0 \\ \gamma v/c & 0 & 0 & \gamma \end{pmatrix} \end{aligned} \quad (2.13)$$

where $\gamma = (1 - v^2/c^2)^{-1/2}$, v is the collision velocity (with the z axis chosen along the beam direction) and $b = (0, b_x, b_y, 0)$ is the impact parameter. Then

$$\begin{aligned} \frac{1}{c} (q'_s(x'), \hat{S} p_\sigma(x)) &= \frac{1}{(2\pi)^4} \frac{1}{c} \int d\mathbf{x}' c dt' u_q^{(s)+} e^{-iq\mathbf{x}'} e^{i\delta_s \omega_q t'} \sqrt{\frac{1+\gamma}{2}} \left(1 - \frac{\gamma v/c}{1+\gamma} \alpha_z \right) \\ &\quad \times u_p^{(\sigma)} e^{ip_\perp(x'_\perp + b)} e^{ip_z \gamma(z' + vt')} e^{-i\delta_\sigma \omega_p \gamma(t' + v z'/c^2)} \end{aligned}$$

$$\begin{aligned}
&= \sqrt{\frac{1+\gamma}{2}} \left[u_q^{(s)+} \left(1 - \frac{\gamma v/c}{1+\gamma} \alpha_z \right) u_p^{(\sigma)} \right] e^{i\mathbf{p}_\perp \cdot \mathbf{b}} \delta(\mathbf{p}_\perp - \mathbf{q}_\perp) \\
&\quad \times \delta(\delta_s \omega_q + p_z \gamma v - \gamma \delta_\sigma \omega_p) \delta \left(-q_z + p_z \gamma - \gamma \delta_\sigma \omega_p \frac{v}{c^2} \right). \tag{2.14}
\end{aligned}$$

As concerns the spin sums, it follows from the δ -function in (2.9) that $\delta_s = 1$ since $E'_f + \omega' > 0$ and $\omega_q > 0$. Also from (2.12), $\delta_\sigma > 0$ since $E_i^T, \omega_p > 0$. Therefore, the sums over s and σ run only over the particle states. However, in the scalar product $u_p^{(\sigma)+} \varphi_{i,T}^{(\sigma_i)}(\mathbf{p})$ in (2.12), the antiparticle contribution $\sigma = 3, 4$ is also strongly suppressed because we only consider a light (nonrelativistic) target whose momentum distribution is strongly peaked at $p = 0$ where $u_p^{(\sigma)+} \varphi_{i,T}^{(\sigma_i)}(\mathbf{p})$ is strictly zero for $\sigma = 3, 4$. Therefore, (2.12) would approximately vanish for antiparticle states even without the presence of the δ -function. Hence, after carrying out the ω_p integration (by means of the δ -function), the sum over σ may well be extended up to $\sigma = 4$ such that the completeness relation $\sum_{\sigma=1}^4 u_p^{(\sigma)} u_p^{(\sigma)+} = 1$ can be used. Then M turns into

$$M = \frac{\sqrt{2\pi}}{\gamma} \sqrt{\frac{1+\gamma}{2}} \left[u_q^{(s)+} \left(1 - \frac{\gamma v/c}{1+\gamma} \alpha_z \right) \varphi_{i,T}^{(\sigma_i)}(\mathbf{p}) \right] e^{i\mathbf{q}_\perp \cdot \mathbf{b}} \delta \left(\delta_s \omega_q - \gamma E_i^T + v \left[\gamma E_i^T \frac{v}{c^2} + q_z \right] \right) \tag{2.15}$$

where $\mathbf{p} = (\mathbf{p}_\perp, p_z)$ with $\mathbf{p}_\perp = \mathbf{q}_\perp$ and $p_z = E_i^T v/c^2 + q_z/\gamma$. Collecting results, the transition amplitude (2.8) is

$$\begin{aligned}
a_{fi}^{\text{IA}} &= \frac{2\pi i}{\gamma} \sqrt{\frac{1+\gamma}{2}} \mathcal{A}'_\lambda \sum_{s=1}^2 \int d\mathbf{q} e^{i\mathbf{q}_\perp \cdot \mathbf{b}} \mathbf{W}_{\text{rad}}(\sigma_f, s, \mathbf{q}) \\
&\quad \times \left[u_q^{(s)+} \left(1 - \frac{\gamma v/c}{1+\gamma} \alpha_z \right) \varphi_{i,T}^{(\sigma_i)}(\mathbf{p}) \right] \delta(E'_f + \omega' - E_i^T/\gamma + q_z v). \tag{2.16}
\end{aligned}$$

2.2. Cross section

In order to obtain the total cross section for target ionization from an initial state i with simultaneous photon emission one has to integrate over impact parameter and sum over the unobserved final states. If one does not fix the spin state of the initial electron one must, in addition, average over these states. If calculated in the projectile frame of reference, one thus needs to evaluate

$$\sigma = \int \frac{d\mathbf{k}'}{\omega'/c^2} \int \frac{d\mathbf{k}'_f}{E'_f/c^2} \frac{1}{2} \sum_{\sigma_i} \sum_{\lambda, \sigma_f} \int d^2\mathbf{b} \left| \sqrt{\frac{\omega'}{c^2} \frac{E'_f}{c^2}} a_{fi}^{\text{IA}} \right|^2. \tag{2.17}$$

The sum over the final states involves a sum over the spin projections σ_f , the polarization directions e_λ as well as the momenta of the photon (\mathbf{k}') and the emitted electron (\mathbf{k}'_f). The volume elements are written in the relativistically invariant form (Bjorken and Drell 1964, p 124) which simplifies the conversion to the laboratory frame. The corresponding Lorentz transformation for the 4-momenta is

$$\begin{pmatrix} E/c \\ k_x \\ k_y \\ k_z \end{pmatrix} = \Gamma \begin{pmatrix} E'/c \\ k'_x \\ k'_y \\ k'_z \end{pmatrix} \tag{2.18}$$

with Γ from (2.13). The inverse transformation is obtained by replacing v with $-v$ in Γ . One derives the relations

$$\omega' = \gamma \omega \left(1 - \frac{v}{c} \cos \theta \right), \quad E'_f = \gamma (E_f - v k_f \cos \vartheta_f) \tag{2.19}$$

where $\theta = \angle(\mathbf{k}, \mathbf{v})$ is the photon emission angle and $\vartheta_f = \angle(\mathbf{k}_f, \mathbf{v})$ is the electron emission angle (in the target frame of reference). With $\frac{d\mathbf{k}'}{\omega'/c^2} = \frac{d\mathbf{k}}{\omega/c^2}$, $\frac{d\mathbf{k}'_f}{E'_f/c^2} = \frac{d\mathbf{k}_f}{E_f/c^2}$ and $d\mathbf{k} = \frac{\omega^2}{c^3} d\omega d\Omega$, $d\mathbf{k}_f = \frac{k_f E_f}{c^2} dE_f d\Omega_f$ one obtains the fourfold differential cross section for electron emission with energy E_f into the solid angle $d\Omega_f$ accompanied by the emission of a photon with energy ω into the solid angle $d\Omega$:

$$\begin{aligned} \frac{d^4\sigma}{dE_f d\Omega_f d\omega d\Omega} &= \frac{k_f \omega \omega' E'_f}{2c^5} \sum_{\lambda, \sigma_i, \sigma_f} \int d^2\mathbf{b} |a_{fi}^{JA}|^2 \\ &= \frac{(2\pi)^4 (1+\gamma)}{4c^5 v} k_f \omega^2 \left(1 - \frac{v}{c} \cos\theta\right) (E_f - v k_f \cos\vartheta_f) S \\ S &= \sum_{\lambda, \sigma_i, \sigma_f} \int d\mathbf{q} \delta(E'_f + \omega' - E_i^T/\gamma + q_z v) \\ &\quad \times \left| A'_\lambda \sum_{s=1}^2 \mathbf{W}_{rad}(\sigma_f, s, q) \left[u_q^{(s)+} \left(1 - \frac{\gamma v/c}{1+\gamma} \alpha_z\right) \varphi_{i,T}^{(\sigma_i)}(\mathbf{p}) \right] \right|^2. \end{aligned} \quad (2.20)$$

The polarization vectors of the photon are perpendicular to its wavevector, so with $\mathbf{k}' = (k' \sin\theta', 0, k' \cos\theta')$ one can choose

$$\mathbf{e}_{\lambda_1} = (0, 1, 0), \quad \mathbf{e}_{\lambda_2} = (-\cos\theta', 0, \sin\theta'). \quad (2.21)$$

These vectors can be converted to the target frame of reference by means of $\cos\theta' = (\cos\theta - \frac{v}{c}) / (1 - \frac{v}{c} \cos\theta)$, $\sin\theta' = \sin\theta / (\gamma(1 - \frac{v}{c} \cos\theta))$ which are derived from (2.18).

2.3. Approximations

In this section we describe the approximations used for the electronic wavefunctions. Since the exact relativistic wavefunctions do not allow for a representation of the matrix elements in closed form, semirelativistic wavefunctions are used which are exact up to first order in Z/c with Z the respective nuclear charge.

For the bound states, this semirelativistic approximation leads to the Darwin functions (Davidović *et al* 1978). These functions provide an excellent description for the light targets considered here. In momentum space a target state characterized by the quantum numbers j_i, l_i, m_i and $s_i = 1/2$ is given by

$$\begin{aligned} \varphi_{i,T}^{(sign m_i)}(\mathbf{p}) &= N_i^T \sum_{m_i, m_s} (l_i m_i s_i m_s | j_i m_i) a_i^{(sign m_s)}(\mathbf{p}) \tilde{\varphi}_{i,T}(\mathbf{p}) \\ N_i^T &= \left[1 + \left(\frac{Z_T \mu}{n_i} \right)^2 \right]^{-1/2} \\ a_i^{(+)}(\mathbf{p}) &= \begin{pmatrix} 1 \\ 0 \\ \mu p_z \\ \mu p_+ \end{pmatrix}, \quad a_i^{(-)}(\mathbf{p}) = \begin{pmatrix} 0 \\ 1 \\ \mu p_- \\ -\mu p_z \end{pmatrix} \end{aligned} \quad (2.22)$$

with $p_\pm = p_x \pm i p_y$, $\mu = c/(E_i^T + mc^2)$ and $\tilde{\varphi}_{i,T}(\mathbf{p})$ the nonrelativistic bound-state momentum-space wavefunction characterized by n_i, l_i, m_i . In the case $l_i = 0$, the sum in (2.22) consists of a single term, such that the factor of (2.20) in square brackets reduces to

$$\left[u_q^{(s)+} \left(1 - \frac{\gamma v/c}{1+\gamma} \alpha_z\right) a_i^{(\sigma_i)}(\mathbf{p}) \right] N_i^T \tilde{\varphi}_{i,T}(\mathbf{p}). \quad (2.23)$$

The function $\tilde{\varphi}_{i,T}$ is independent of s and hence can be taken outside the spin sum in (2.20). For $l_i \neq 0$ an average over j_i and m_i may be carried out since, for light targets, the j_i subshells are

approximately degenerate. According to Jakubaša-Amundsen (1997) this leads to the simple replacement in (2.23)

$$|\tilde{\varphi}_{i,T}(\mathbf{p})|^2 \longrightarrow \frac{1}{2l_i + 1} \sum_{m_i} |\tilde{\varphi}_{l_i, m_i, T}(\mathbf{p})|^2. \quad (2.24)$$

The projectile scattering states are described in terms of the semirelativistic Sommerfeld–Maue wavefunctions. Despite their approximate nature for high- Z atoms, they have been successfully applied to explain measured bremsstrahlung cross sections even for $Z = 79$ (Geisenhofer and Nakel 1996, Shaffer *et al* 1996). The Sommerfeld–Maue functions are defined in terms of derivatives of confluent hypergeometric functions (see e.g. Eichler 1990, p 187)

$$\begin{aligned} \psi_{q,P}^{(s')}(\mathbf{x}') &= N_q e^{iq\mathbf{x}'} \left(1 - \frac{ic}{2E_q} \boldsymbol{\alpha} \nabla \right) {}_1F_1(i\eta_q, 1, i(qr' - \mathbf{q}\mathbf{x}')) u_q^{(s)} \\ N_q &= \frac{1}{(2\pi)^{3/2}} e^{\pi\eta_q/2} \Gamma(1 - i\eta_q), \quad u_q^{(+)} = C_q \begin{pmatrix} 1 \\ 0 \\ vq_z \\ vq_+ \end{pmatrix}, \quad u_q^{(-)} = C_q \begin{pmatrix} 0 \\ 1 \\ vq_- \\ -vq_z \end{pmatrix} \end{aligned} \quad (2.25)$$

with

$$\begin{aligned} \eta_q &= \frac{Z_P E_q}{qc^2}, & r' &= |\mathbf{x}'|, & C_q &= \left(\frac{E_q + c^2}{2E_q} \right)^{1/2}, \\ v &= c/(E_q + c^2), & q_{\pm} &= q_x \pm iq_y, & E_q &= (q^2 c^2 + c^4)^{1/2}. \end{aligned}$$

With the abbreviations $F_q = {}_1F_1(i\eta_q, 1, i(qr' - \mathbf{q}\mathbf{x}'))$ and $F_k = {}_1F_1(i\eta_f, 1, i(k'_f r' + \mathbf{k}'_f \mathbf{x}'))$ the radiation matrix element (2.10) simplifies to

$$\begin{aligned} W_{rad}(\sigma_f, s, q) &= N_q N_f u_{k'_f}^{(\sigma_f)+} \left[\int d\mathbf{x}' M_{kq}(\mathbf{x}') \right] u_q^{(s)} \\ M_{kq}(\mathbf{x}') &= e^{-ik'_f \mathbf{x}'} F_k \boldsymbol{\alpha} e^{i(q-k')\mathbf{x}'} F_q + e^{-ik'_f \mathbf{x}'} \frac{ic}{2E_f} (\boldsymbol{\alpha} \nabla F_k) \boldsymbol{\alpha} e^{i(q-k')\mathbf{x}'} F_q \\ &\quad - e^{-ik'_f \mathbf{x}'} F_k \boldsymbol{\alpha} e^{i(q-k')\mathbf{x}'} \frac{ic}{2E_q} (\boldsymbol{\alpha} \nabla F_q) \end{aligned} \quad (2.26)$$

where a fourth term containing the product of derivatives has been dropped for consistency with a first-order approximation in Z_P/c (Elwert and Haug 1969). N_f is identical to N_q but for the replacement of η_q by $\eta_f = Z_P E_f / k'_f c^2 \approx Z_P / k'_f$ for small k'_f . For the further evaluation the identity is used:

$$\nabla_{\mathbf{x}'} {}_1F_1(i\eta_q, 1, i(s_0 r' - \mathbf{s}_0 \mathbf{x}')) = -\frac{s_0}{r'} \nabla_{\mathbf{s}_0} {}_1F_1(i\eta_q, 1, i(s_0 r' - \mathbf{s}_0 \mathbf{x}')) \quad (2.27)$$

such that the radiation matrix element can be written in terms of two integrals:

$$\begin{aligned} I_0 &= \int d\mathbf{x}' e^{ip_0 \mathbf{x}'} F_k F_q \\ I_1(\mathbf{s}_0) &= \nabla_{\mathbf{s}_0} \int d\mathbf{x}' \frac{1}{r'} {}_1F_1(i\eta_q, 1, i(s_0 r' - \mathbf{s}_0 \mathbf{x}')) e^{ip_0 \mathbf{x}'} F_k \end{aligned} \quad (2.28)$$

where $\mathbf{p}_0 = \mathbf{q} - \mathbf{k}' - \mathbf{k}'_f$ is introduced and \mathbf{s}_0 must ultimately be replaced by \mathbf{q} . Both integrals can be evaluated analytically with the help of the Nordsieck (1954) formula:

$$\begin{aligned} I_0 &= -\lim_{\epsilon \rightarrow 0} \frac{\partial}{\partial \epsilon} W(\epsilon), \quad I_1(\mathbf{s}_0) = \lim_{\epsilon \rightarrow 0} \nabla_{\mathbf{s}_0} W(\epsilon) \\ W(\epsilon) &= \int d\mathbf{x} \frac{1}{r} {}_1F_1(i\eta_q, 1, i(s_0 r - \mathbf{s}_0 \mathbf{x})) e^{ip_0 \mathbf{x}} e^{-\epsilon r} {}_1F_1(i\eta_f, 1, i(k'_f r + \mathbf{k}'_f \mathbf{x})) \\ &= \frac{2\pi}{\tilde{\alpha}} e^{-\pi\eta_q} \left(\frac{\tilde{\alpha}}{\tilde{\gamma}} \right)^{i\eta_q} \left(\frac{\tilde{\gamma} + \tilde{\delta}}{\tilde{\gamma}} \right)^{-i\eta_f} {}_2F_1 \left(1 - i\eta_q, i\eta_f, 1, \frac{\tilde{\alpha}\tilde{\delta} - \tilde{\beta}\tilde{\gamma}}{\tilde{\alpha}(\tilde{\gamma} + \tilde{\delta})} \right) \end{aligned} \quad (2.29)$$

with $\tilde{\alpha} = \frac{1}{2}(p_0^2 + \epsilon^2)$, $\tilde{\beta} = \mathbf{k}'_f \mathbf{p}_0 - i\epsilon \mathbf{k}'_f$, $\tilde{\gamma} = s_0 \mathbf{p}_0 + i\epsilon s_0 - \tilde{\alpha}$, $\tilde{\delta} = s_0 \mathbf{k}'_f + s_0 \mathbf{k}'_f - \tilde{\beta}$ and ${}_2F_1$ is a hypergeometric function. For the second integral one obtains

$$\begin{aligned} I_1(\mathbf{q}) = & 2\pi e^{-\pi\eta_q} \tilde{\alpha}^{i\eta_q-1} \tilde{\gamma}^{i\eta_f-i\eta_q-1} (\tilde{\gamma} + \tilde{\delta})^{-i\eta_f-1} \left\{ {}_2F_1\left(1 - i\eta_q, i\eta_f, 1, \frac{\tilde{\alpha}\tilde{\delta} - \tilde{\beta}\tilde{\gamma}}{\tilde{\alpha}(\tilde{\gamma} + \tilde{\delta})}\right) \right. \\ & \times \left[-i\eta_f \tilde{\gamma} \left(\mathbf{p}_0 + \mathbf{k}'_f \frac{\mathbf{q}}{q} + \mathbf{k}'_f \right) + i(\eta_f - \eta_q) \mathbf{p}_0 (\tilde{\gamma} + \tilde{\delta}) \right] \\ & + {}_2F_1\left(2 - i\eta_q, 1 + i\eta_f, 2, \frac{\tilde{\alpha}\tilde{\delta} - \tilde{\beta}\tilde{\gamma}}{\tilde{\alpha}(\tilde{\gamma} + \tilde{\delta})}\right) i\eta_f (1 - i\eta_q) \\ & \left. \times \frac{(\tilde{\alpha} + \tilde{\beta})\tilde{\gamma}}{\tilde{\alpha}(\tilde{\gamma} + \tilde{\delta})} \left[\tilde{\gamma} \mathbf{k}'_f \frac{\mathbf{q}}{q} + \tilde{\gamma} \mathbf{k}'_f - \tilde{\delta} \mathbf{p}_0 \right] \right\}. \end{aligned} \quad (2.30)$$

I_0 is calculated along the same lines (Jakubaša-Amundsen 1983). The radiation matrix element (2.26) is proportional to

$$I := \int d\mathbf{x}' M_{kq}(\mathbf{x}') = \left[1 + \frac{c}{2E'_f} (\boldsymbol{\alpha} \mathbf{p}_0) \right] \boldsymbol{\alpha} I_0 + \frac{icq}{2} \left[\frac{2}{E'_f} I_1(\mathbf{q}) - \left(\frac{1}{E'_f} - \frac{1}{E_q} \right) \boldsymbol{\alpha} (\boldsymbol{\alpha} I_1(\mathbf{q})) \right]. \quad (2.31)$$

Introducing cylindrical coordinates (q_\perp, φ_q, q_z) for \mathbf{q} , the integral over q_z becomes trivial and the cross section (2.20) turns into

$$\begin{aligned} \frac{d^4\sigma}{dE_f d\Omega_f d\omega d\Omega} = & \frac{(2\pi)^4 (1 + \gamma)}{4c^5 v^2} k_f \omega^2 \left(1 - \frac{v}{c} \cos\theta \right) (E_f - vk_f \cos\vartheta_f) |N_i^T N_f|^2 \\ & \times \int_0^\infty q_\perp dq_\perp \left| \tilde{\varphi}_{i,T} \left(\mathbf{q}_\perp, E_i^T \frac{v}{c^2} + \frac{q_z}{\gamma} \right) \right|^2 |N_q|^2 \int_0^{2\pi} d\varphi_q \\ & \times \sum_{\lambda=1}^2 \sum_{\sigma_i, \sigma_f=1}^2 \left| u_{k'_f}^{(\sigma_f)+} (\mathbf{A}'_\lambda \mathbf{I}) \left(\sum_{s=1}^2 u_q^{(s)} u_q^{(s)+} \right) \left(1 - \frac{\gamma v/c}{1 + \gamma} \alpha_z \right) a_i^{(\sigma_i)} \right. \\ & \left. \times \left(\mathbf{q}_\perp, E_i^T \frac{v}{c^2} + \frac{q_z}{\gamma} \right) \right|^2, \quad q_z = -\frac{1}{v} (E'_f + \omega' - E_i^T / \gamma). \end{aligned} \quad (2.32)$$

One has $|2\pi N_f|^2 = \eta_f / (1 - e^{-2\pi\eta_f})$ and $|2\pi N_q|^2 = \eta_q / (1 - e^{-2\pi\eta_q})$. Note that the differential cross section (2.32) depends both on the polar (ϑ_f) and azimuthal angle (φ_f) of \mathbf{k}_f , because a plane is defined by the outgoing electron and photon which destroys the symmetry with respect to the beam axis (except for $\vartheta_f = 0^\circ, 180^\circ$).

3. Cross section analysis and results

The fourfold differential cross section for radiative ionization is calculated from (2.32) without further approximations. The hypergeometric functions occurring in the radiation matrix elements are obtained by means of their series expansion since the argument $z = (\tilde{\alpha}\tilde{\delta} - \tilde{\beta}\tilde{\gamma}) / (\tilde{\alpha}(\tilde{\gamma} + \tilde{\delta})) \ll 1$ in the region of interest. The matrix multiplications and the spin sums are evaluated numerically. In the case of nonhydrogenic targets, the nonrelativistic part $\tilde{\varphi}_{l, m_l, T}$ of the Darwin functions is taken as a Hartree–Fock single-particle wavefunction which is Fourier transformed with the method of fast Bessel transforms (Talman 1978) as described in Jakubaša-Amundsen (1997). Also, experimental binding energies are used.

3.1. Structure of the differential cross section

The prominent feature of the RI cross section differential in energy and angle of the emitted electron is the cusp at $E'_f = c^2$ corresponding to a laboratory-frame kinetic energy of

$E_{f,kin} = E_f - c^2 = \gamma E'_f - c^2 = c^2(\gamma - 1)$. It arises from the divergence of the final-state normalization factor N_f when $\eta_f \approx Z_p/k'_f \rightarrow \infty$ as $k'_f \rightarrow 0$.

However, the cusp shape depends strongly on the projectile and target. For the sake of a detailed analysis, peaking approximations are introduced to make the theory more transparent.

For the light targets considered here, the spherically (or spherically averaged) initial-state density $|\tilde{\varphi}_{i,T}(\mathbf{q}_\perp, E_i^T v/c^2 + q_z/\gamma)|^2$ is strongly peaked at zero momentum, i.e. at $q_\perp = 0$ and $q_z = -\gamma E_i^T v/c^2 \approx -\gamma v$ for $E_i^T \approx c^2$. Due to the photon degrees of freedom, q_z is not fixed by the energy-conserving δ -function. Taking the slowly varying remainder of the \mathbf{q} integrand outside the integral at $\mathbf{q} = (0, q_{z0})$ with $q_{z0} = -\gamma E_i^T v/c^2$, one sees that the differential cross section (2.20) or (2.32) becomes proportional to the target Compton profile J_i :

$$\begin{aligned} \int d\mathbf{q} \delta(E'_f + \omega' - E_i^T/\gamma + q_z v) |\tilde{\varphi}_{i,T}(\mathbf{q}_\perp, E_i^T v/c^2 + q_z/\gamma)|^2 \\ = \frac{1}{v} J_i(E_i^T v/c^2 + q_z/\gamma) = \frac{1}{v} J_i\left(E_i^T/v - \frac{1}{\gamma v}(E'_f + \omega')\right). \end{aligned} \quad (3.1)$$

From this it follows that the photon spectrum is peaked at $\omega' = \omega'_{peak} = \gamma E_i^T - E'_f$, the peak shape being determined by the momentum distribution of the bound electron in its initial state. A similar dependence on the Compton profile of the initial state is also known from REC peak studies (see, e.g., Stöhlker *et al* 1998). Figure 1 shows the photon spectrum from $U^{92+} + H$ collisions at an electron momentum slightly above the cusp for two collision velocities, $v = 97.7$ and 58.7 . The spectrum is plotted versus $(\omega - \omega_{peak})/v$ which is the argument of J_i when transformed to the target frame at the photon angle $\theta = 90^\circ$ ($\omega = \omega'/\gamma$). It is evident from figure 1 that this scaling of the Compton profile is valid for the differential cross section.

If the photon frequency is fixed at, say, $\omega' = \omega'_{peak}(E'_f = c^2)$ but E'_f is varied, it follows from (3.1) that the electron spectrum is also sensitive to the target Compton profile. This is shown in figure 2 where the electron spectrum resulting from $400 \text{ MeV amu}^{-1} U^{92+} + N$ collisions is plotted. The narrow cusp at $E_{f,kin} = 217.9 \text{ keV}$ is superimposed on a broad peak which mirrors the momentum distribution of the nitrogen subshells.

In REC studies, the angular distribution of the emitted photons has attained a great deal of interest. While nonrelativistically it shows a $\sin^2 \theta$ dependence, the relativistic theory for REC into the inner shells still gives an approximate $\sin^2 \theta$ variation, resulting from mutual cancellation of retardation and Lorentz transformation effects (Spindler *et al* 1979, Stöhlker *et al* 1997). Figure 3 depicts the angular photon distribution for radiative ionization at electron energies slightly above and below the cusp. The deviation from a sinusoidal shape is quite significant. Apart from finite cross sections at 0° and 180° which result from contributions of all multiplicities to the RI transition amplitude, the photon distribution is peaked at angles $< 90^\circ$ for 216 keV electrons, while the peak is shifted to backward angles for energies beyond the cusp. A comparison of the REC spectra obtained with Sommerfeld–Maue functions and with exact relativistic wavefunctions, respectively (Eichler 1990), indicates that the strong peak shift to the backward direction may partly be due to the use of inaccurate wavefunctions. This conjecture is supported by bremsstrahlung investigations (Tseng and Pratt 1971), but the difference between results with the two types of wavefunctions is considerably smaller in that case.

3.2. Cusp cross section

In order to compare with experiment, the fourfold differential RI cross section has to be convoluted with the detector resolution. Particularly crucial is the averaging over the angular

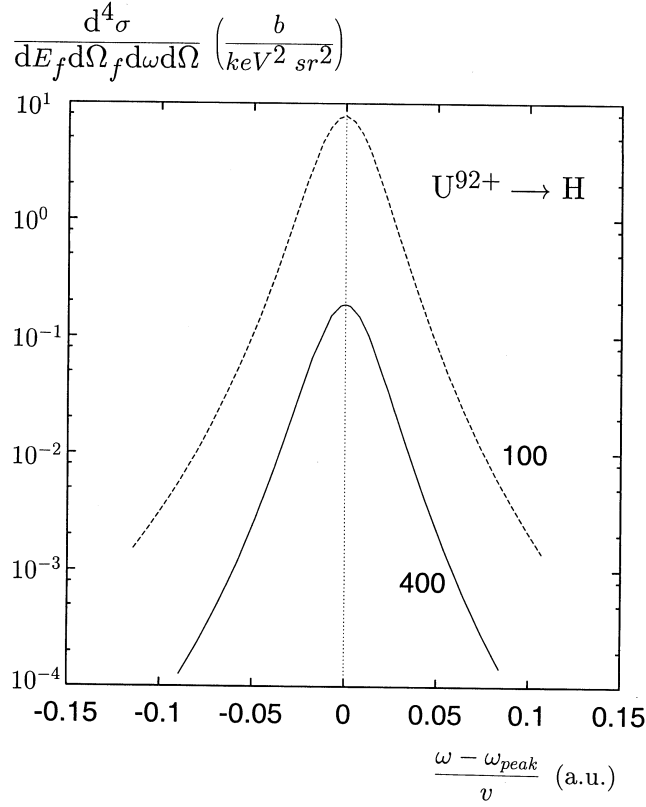


Figure 1. Fourfold differential cross section for RI from 100 and 400 MeV amu⁻¹ U⁹²⁺ + H collisions for forward electron emission ($\vartheta_f = 0^\circ$) as a function of scaled photon energy ω . The photon emission angle is $\theta = 90^\circ$, kinetic electron energy $E_{f,kin} = E_f - mc^2 = 55$ keV (upper curve) and 220 keV (lower curve). The respective peak frequencies are $\omega_{peak} = 49.22$ and 152.75 keV.

resolution of the electron spectrometer. Let $\pm\theta_0$ be the angular acceptance around $\vartheta_f = 0$. Then one defines

$$\left\langle \frac{d^4\sigma}{dE_f d\Omega_f d\omega d\Omega} \right\rangle_{\theta_0} = \frac{1}{1 - \cos\theta_0} \int_0^{\theta_0} \sin\vartheta_f d\vartheta_f \left(\frac{1}{\pi} \int_0^\pi d\varphi_f \frac{d^4\sigma}{dE_f d\Omega_f d\omega d\Omega} \right) \quad (3.2)$$

where the expression in brackets on the rhs provides an additional averaging over the azimuthal electron angle φ_f if the emission direction of the electron (with respect to the photon) is not specified experimentally for $0 < \vartheta_f \leq \theta_0$. Figure 4 shows the cusp spectrum from 100 MeV amu⁻¹ U⁹²⁺ + H collisions. The fourfold differential cross section at forward emission, both averaged and non-averaged, are plotted. Also given is the cross section divided by the normalization factor $|2\pi N_f|^2$ in order to display the background spectrum. The strong asymmetry with respect to the cusp energy will be discussed in the next section.

In figure 5 the velocity dependence of the peak value of the averaged cross section is displayed. A strong decrease with γv is found, which is similar for the two projectiles investigated, U⁹²⁺ and Kr³⁶⁺. There is an increase of the peak value with projectile charge according to Z_p^λ with $2.1 \lesssim \lambda \lesssim 2.2$. This should not be confused with the Z_p^2 dependence of the first Born approximation for (radiationless) target ionization since, in the present theory, the projectile field is included to all orders in the final electronic state.

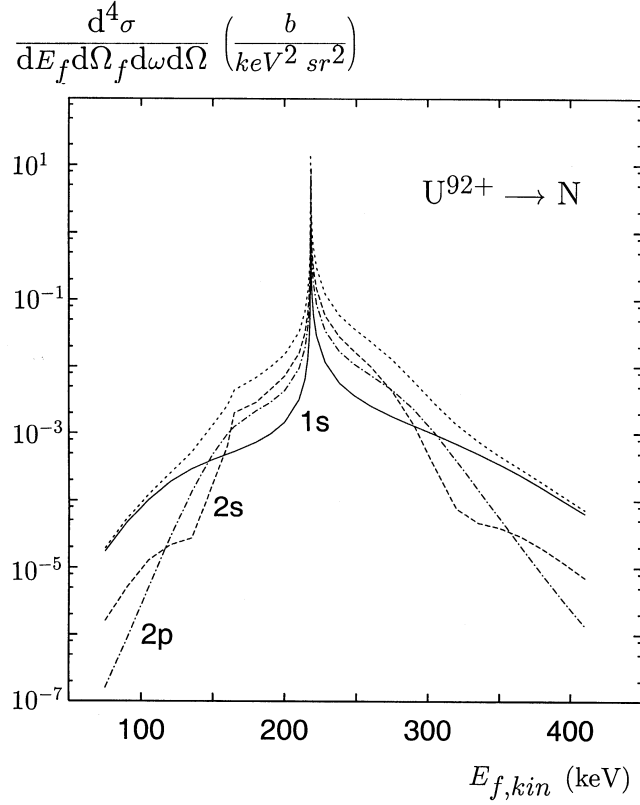


Figure 2. Fourfold differential cross section for RI from $400 \text{ MeV amu}^{-1} \text{U}^{92+} + \text{N}$ collisions at forward emission ($\vartheta_f = 0^\circ$) as a function of kinetic electron energy $E_{f,kin}$. Shown are the contributions from the nitrogen 1s electrons (—), 2s electrons (---), 2p electrons (— · —) and their sum (····). The photon parameters are $\theta = 90^\circ$, $\omega = 152.75 \text{ keV}$ which is the peak frequency at the cusp position.

3.3. Cusp asymmetry

As discussed in Jakubaša-Amundsen (1983), the cusp asymmetry in the case of (radiationless) electron capture to continuum arises from a discontinuity of the matrix element describing inelastic electron scattering from the projectile field, when ϑ'_f switches from 0° to 180° in the limit $k_f \rightarrow 0$. In first-order Born theory, where the ‘incoming’ electron is described by a plane wave (instead of a projectile scattering eigenstate), this discontinuity is only contained in a phase factor and therefore is not visible in the cross section. For the cusp asymmetry to occur, a higher-order approximation is required. Experimentally measured cusp asymmetries are thus a sensitive test of theory.

In the case of RI, the pathological matrix element is \mathbf{W}_{rad} , or more precisely, the hypergeometric functions contained in I_0 and I_1 from (2.29) and (2.30). In the limit $k'_f \rightarrow 0$, i.e. $\eta_f \rightarrow \infty$, the hypergeometric function ${}_2F_1(a, i\eta_f + l, c, z)$ turns into the confluent hypergeometric function ${}_1F_1(a, c, i\eta_f z)$ if a, l, c are constants and $z \sim k'_f$. We will show that the argument $i\eta_f z = i\eta_f \frac{\tilde{\alpha}\tilde{\delta} - \tilde{\beta}\tilde{\gamma}}{\tilde{\alpha}(\tilde{\gamma} + \tilde{\delta})}$ still depends on the electron emission angle ϑ'_f . With this aim the peaking approximations from section 3.1 are applied. Recalling these results (with

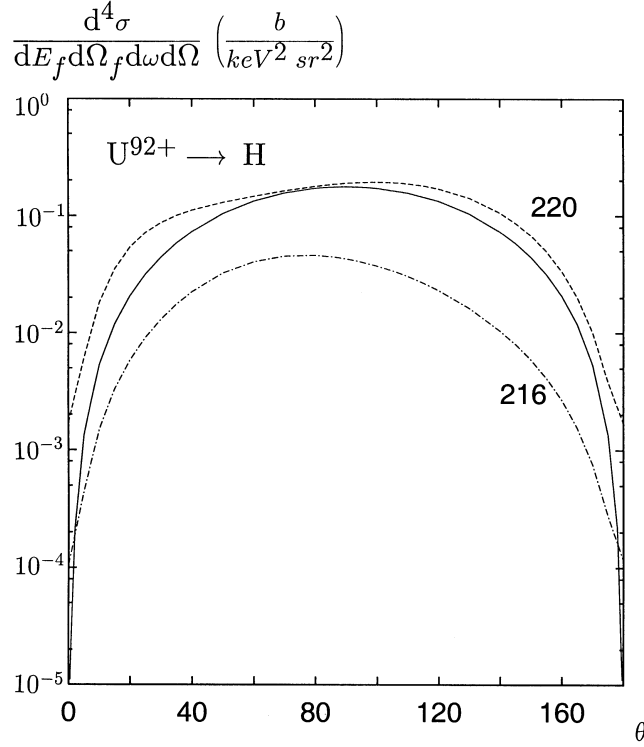


Figure 3. Fourfold differential cross section for RI from 400 MeV $\text{amu}^{-1}\text{U}^{92+} + \text{H}$ collisions as a function of photon angle θ for forward electron emission ($\vartheta_f = 0^\circ$) at two energies $E_{f,kin} = 216$ keV (— · —) and 220 keV (---). The photon frequency is $\omega = 152.75$ keV. Also shown is the $\sin^2\theta$ distribution (—) normalized at $\theta = 90^\circ$ to the corresponding cross section at the higher electron energy.

$E_i^T \approx c^2$) and considering only electron emission parallel or antiparallel to the beam direction, one has

$$\begin{aligned}
 \mathbf{k}'_f &= \pm \epsilon \mathbf{e}_z, & \epsilon &\rightarrow +0, & E'_f &\approx c^2 \\
 \mathbf{q} &\approx -\gamma \mathbf{v}, & \omega' &\approx (\gamma - 1)c^2, \\
 \mathbf{k}' &= k' \mathbf{e}'_k, & k' &= \omega'/c \approx (\gamma - 1)c, & \mathbf{e}'_k &= (\sin \theta', 0, \cos \theta')
 \end{aligned} \tag{3.3}$$

where $+\epsilon$ corresponds to $\vartheta'_f = 0$ and $-\epsilon$ to $\vartheta'_f = 180^\circ$.

Without loss of generality the quantities entering into the argument z can be assumed real (i.e. their tiny imaginary part is disregarded). Also, k'_f is set equal to zero in \mathbf{p}_0 from (2.28). Then one has

$$\begin{aligned}
 \tilde{\alpha} &\approx \frac{1}{2}\gamma^2 v^2 + \frac{1}{2}(\gamma - 1)^2 c^2 + \gamma(\gamma - 1)vc \cos \theta' \\
 \tilde{\beta} &\approx \mp \epsilon(\gamma v + (\gamma - 1)c \cos \theta') \\
 \tilde{\gamma} &\approx \frac{1}{2}\gamma^2 v^2 - \frac{1}{2}(\gamma - 1)^2 c^2 \\
 \tilde{\delta} &\approx \epsilon(\gamma v \pm (\gamma - 1)c \cos \theta')
 \end{aligned} \tag{3.4}$$

where the sign \pm relates to the sign of ϵ in (3.3). One has $\tilde{\alpha} > 0$ and, since $(\gamma - 1)c < \gamma v$ for $v < c$ also $\tilde{\gamma}, \tilde{\delta} > 0$ while $\tilde{\beta} < 0$ for forward emission ($\vartheta'_f = 0$) and $\tilde{\beta} > 0$ for backward emission ($\vartheta'_f = 180^\circ$). In the weak relativistic limit, $\gamma - 1 < 0.1$, one may disregard the

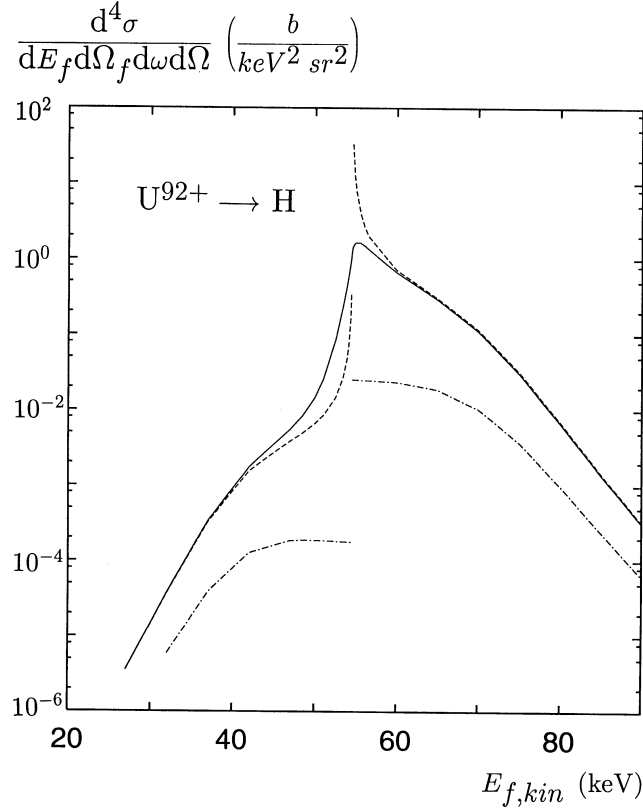


Figure 4. Fourfold differential cross section for RI from 100 MeV amu $U^{92+} + H$ collisions for forward electron emission as a function of kinetic electron energy. Besides the cross section for $\vartheta_f = 0^\circ$ (---), the cross section averaged over a detector angular acceptance of $0 \pm 1.5^\circ$ according to (3.2) is also shown (—). The chain curve denotes the $\vartheta_f = 0^\circ$ cross section divided by $\eta_f/(1 - e^{-2\pi\eta_f})$. The photon parameters are $\theta = 90^\circ$ and $\omega = 49.22$ keV.

terms $\sim(\gamma - 1)$ which originate from the photon momentum. Then with (3.4) and (2.18)

$$i\eta_f z \approx \begin{cases} \frac{4iZ_P}{\gamma v}, & k_{fz} = \gamma(v + \epsilon) \\ 0, & k_{fz} = \gamma(v - \epsilon). \end{cases} \quad (3.5)$$

There is a discontinuity when passing from $k_f < \gamma v$ to $k_f > \gamma v$, which results in different electron emission intensities.

Equation (3.5) suggests that the cusp asymmetry scales with $4iZ_P/\gamma v$. Figure 6 shows the cusp asymmetry A defined by

$$A = \frac{d^4\sigma_N(\gamma c^2 + \epsilon, 0)}{d^4\sigma_N(\gamma c^2 - \epsilon, 0)} \quad (3.6)$$

where $d^4\sigma_N(E_f, \vartheta_f) = \frac{1}{|N_f|^2} \frac{d^4\sigma}{dE_f d\Omega_f d\omega d\Omega}$ is the cross section without the normalization factor and $\epsilon > 0$ is a small quantity. When $Z_P/\gamma v$ is kept fixed, A varies only within 5% for $11 < Z_P \lesssim 98$, and it has a maximum near $Z_P = 64$. For large γ this scaling is no longer valid and the discontinuity of z (and hence of the differential cross section) will also depend on the emission direction θ' of the photon, cf (3.4). At $Z_P \approx 3$, A is 20% below its maximum

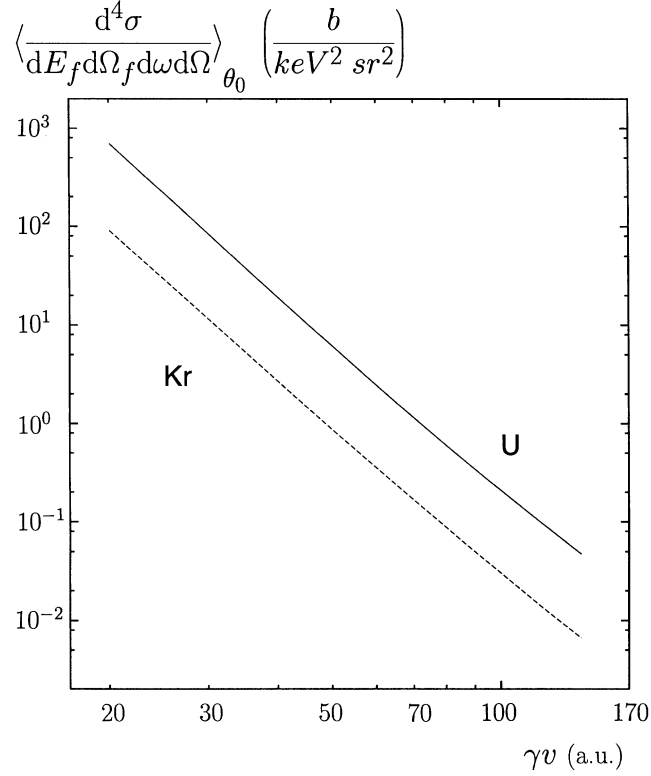


Figure 5. Fourfold differential RI cross section from $U^{92+} + H$ (—) and $Kr^{36+} + H$ (- - -) collisions averaged over the detector resolution $\theta_0 = 1.5^\circ$ for forward electron emission ($\vartheta_f = 0^\circ$) as a function of the collision momentum γv . The photon emission angle is $\theta = 90^\circ$. At each velocity the photon energy is chosen to be the peak energy at the cusp position, and with this ω fixed, E_f is chosen to provide the cross section maximum.

value. The violation of scaling for small Z_P (and hence for small velocities) points to the breakdown of the IA, and consideration of higher-order couplings to the target field will gain importance.

The increase of asymmetry with Z_P at fixed v and its decrease with γv for a given projectile, as suggested by (3.5), is verified in figures 6 and 7.

3.4. Comparison with ECC

In order to compare the RI cusp with the one from radiationless electron capture to continuum, the fourfold differential cross section (2.32) has to be integrated over the photon degrees of freedom. It is convenient to integrate over θ and ω as defined in the target frame of reference. By (2.19) the peak frequency is obtained from $\omega_{peak} = \frac{\omega'_{peak}}{\gamma(1-v/c \cos \theta)}$ where $\omega'_{peak} = \gamma(E_i^T - E_f + vk_f)$ for $\theta_f = 0^\circ$ is independent of θ . The doubly differential RI cross section is calculated from

$$\frac{d^2\sigma}{dE_f d\Omega_f} = 2\pi \int_0^\pi \sin \theta d\theta \int_{\omega_{min}}^{\omega_{peak} + \Delta E} d\omega \frac{d^4\sigma}{dE_f d\Omega_f d\omega d\Omega'} \quad (3.7)$$

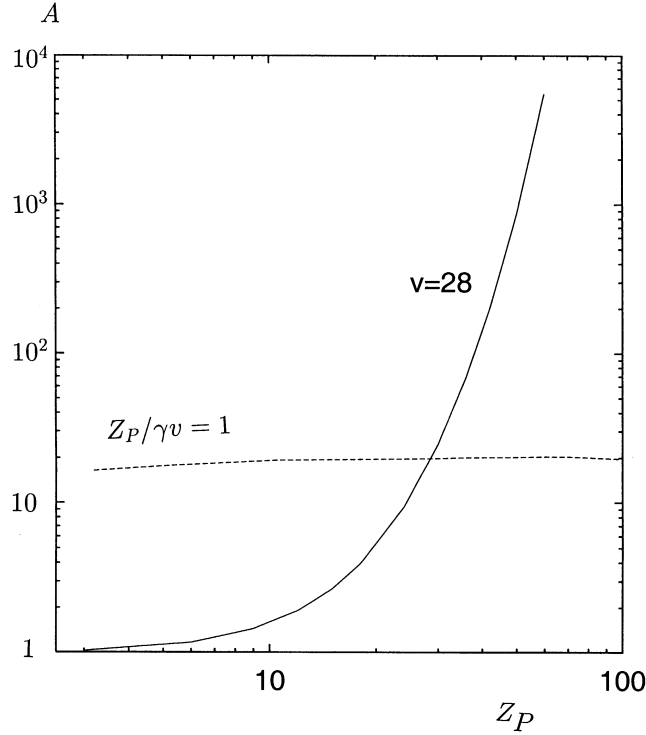


Figure 6. Asymmetry A for collisions of bare projectiles with a hydrogen target as a function of projectile charge Z_P . At each Z_P , v is either taken constant ($v = 28$, —) or chosen such that $Z_P/\gamma v = 1$ (---). ω is taken as the peak frequency at the cusp position (10.77 keV for $v = 28$) and $\theta = 90^\circ$. The electron emission angle is $\vartheta_f = 0^\circ$.

where $\Delta E = \text{constant } v/(1 - \frac{v}{c} \cos \theta)$ with constant ~ 3 as suggested from the argument of the Compton profile for hydrogen, $\frac{1}{\gamma v} (\omega'_{peak} - \omega') = \frac{1}{v} (\omega_{peak} - \omega)(1 - \frac{v}{c} \cos \theta)$, cf (3.1) and the discussion below. Accordingly, $\omega_{min} = \max(0, \omega_{peak} - \Delta E)$.

An estimate of this doubly differential cross section can be obtained from the following consideration. Assuming that (for weakly relativistic systems) the angular distribution follows roughly a $\sin^2 \theta$ dependence, and that the spectrum is exclusively determined by the bound-state Compton profile, one has

$$\begin{aligned} \frac{d^2\sigma}{dE_f d\Omega_f} &\approx 2\pi \left(\int_0^\pi \sin^3 \theta d\theta \right) \left(\frac{1}{J_i(0)} \int_{-\infty}^\infty d\omega J_i \left(\frac{\omega_{peak} - \omega}{v} \right) \right) \\ &\times \frac{d^4\sigma}{dE_f d\Omega_f d\omega d\Omega} \quad (\omega = \omega_{peak}, \theta = 90^\circ). \end{aligned} \quad (3.8)$$

Since in the cusp, $\omega_{peak} = \frac{c^2(\gamma-1)}{\gamma(1-v/c \cos \theta)} > \frac{v^2}{4}$, the lower limit 0 of the ω integral has been replaced by $-\infty$, assuming that $\frac{\omega_{peak}}{v} > \frac{v}{4} \gg \frac{Z_f}{n_i}$ such that the Compton profile is well localized on the positive half-line. For a hydrogen target, $J_i(0) = 8/3\pi$ and the prefactor multiplying the fourfold differential cross section in (3.8) is given by $\pi^2 v$. At the outer wings of the cusp, the approximation (3.8) is, however, rather poor (see figure 8).

Figure 8 compares the electron spectra from 20 MeV $\text{amu}^{-1} \text{Kr}^{36+} + \text{H}$ collisions ($v = 27.9$) at $\vartheta_f = 0$ with and without photon emission. The ECC calculation is nonrelativistic

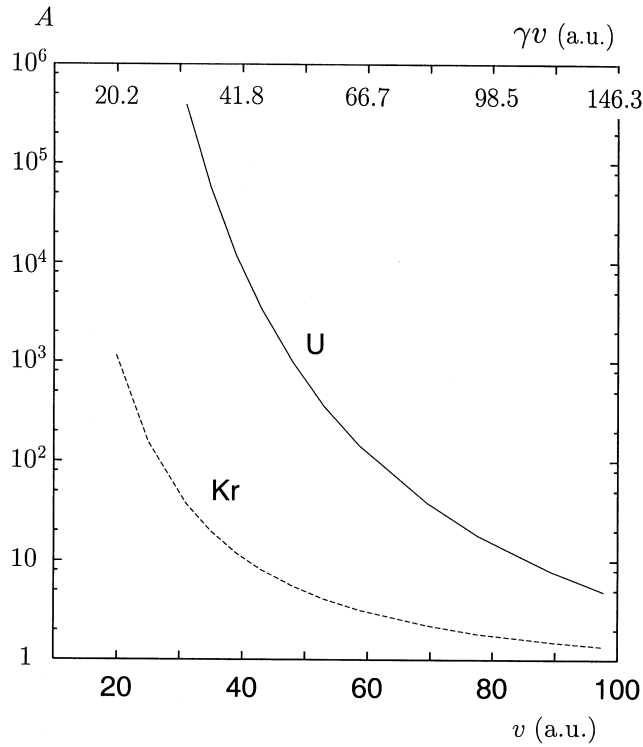


Figure 7. Asymmetry A for collisions of U^{92+} (—) and Kr^{36+} (- - -) with hydrogen as a function of collision velocity (lower scale) and momentum γv (upper scale). The photon frequency is taken as the peak frequency at the cusp position and $\theta = 90^\circ$. The electron emission angle is $\vartheta_f = 0^\circ$.

(Jakubaša-Amundsen 1983) but for this velocity $\gamma = 1.021$ is still close to unity. It is evident that the asymmetries for the two processes are very different. Not only is the RI cusp skewed to the high-energy side whereas the ECC cusp is enhanced at the low-energy side, but the RI cusp asymmetry is also considerably stronger. This is not immediately clear from a mathematical point of view since the discontinuities of the corresponding hypergeometric functions are much alike (Jakubaša-Amundsen 1983).

A physical interpretation is given with the help of figure 9. In the ECC process the cusp electrons originate from high momentum components of the target ($p_z > v/2$), which scatter quasielastically from the projectile. Elastic scattering favours forward angles, such that the electrons are predominantly emitted antiparallel to the beam direction (left panel of figure 9), i.e. $\vartheta'_f = 180^\circ$ or $k_f < \gamma v$. On the other hand, RI is caused by electrons approximately at rest in the target frame (but having kinetic energy $(\gamma - 1)c^2$ in the projectile frame) which are decelerated to low energy ϵ while the excess energy is carried away by the emitted photon. These electrons bounce back from the projectile and are therefore mostly emitted in the beam direction (right panel of figure 9), i.e. $\vartheta'_f = 0$ corresponding to $k_f > \gamma v$.

The doubly differential cross sections near the peak maximum, and therefore also the total cross sections of RI and ECC, are of comparable magnitude for 20 MeV amu^{-1} collision energy. If only electrons are observed, the measured electron yield includes the contributions of both processes, resulting in an RI-type cusp asymmetry which is considerably weakened (figure 8). A first-order Born estimate for the differential RI and ECC cusp cross sections from

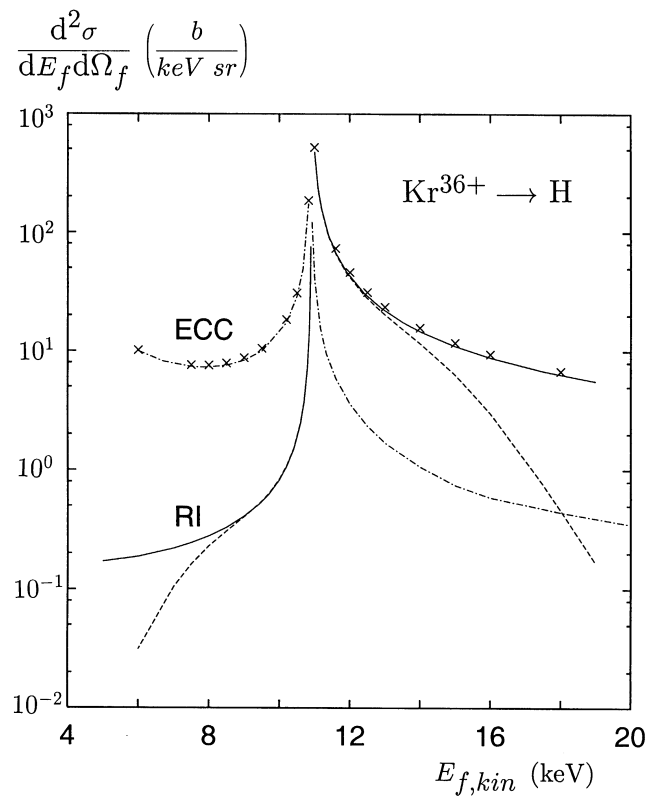


Figure 8. Doubly differential cross section for forward electron emission ($\vartheta_f = 0^\circ$) in $20 \text{ MeV amu}^{-1} \text{ Kr}^{36+} + \text{H}$ collisions as a function of kinetic electron energy. The ECC cross section (\cdots) is taken from Jakubaša-Amundsen (1983). The RI cross section is calculated from (3.7) (—) and from (3.8) (- - -), respectively. The sum of ECC and RI is denoted by ($\times \times \times$).

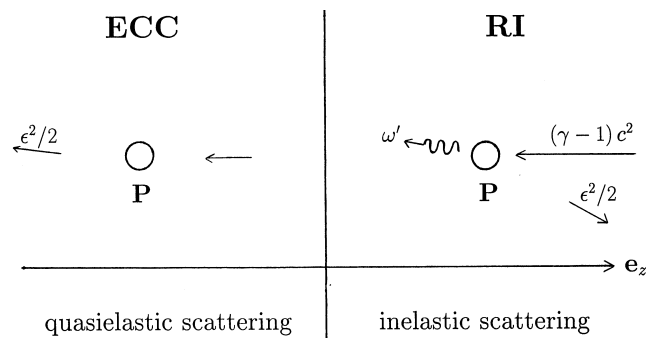


Figure 9. Schematic view of electron scattering from the projectile P during the ECC process (left) and the RI process (right). e_z denotes the beam direction.

$p + \text{H}$ collisions (Miraglia and Garibotti 1985) shows that, at low velocities, ECC is dominant while at high velocity RI will take over, the point of equal magnitude being near 20 MeV. That this is the same energy where the $\text{Kr} + \text{H}$ ECC and RI processes are also of similar importance

[See endnote 1](#)

is, however, considered as fortuitous since ECC has a much stronger Z_P dependence ($\sim Z_P^5$, as conjectured from capture to bound states Jakubaša-Amundsen and Amundsen 1980) than RI ($\sim Z_P^{2.1}$). From figure 5 it follows that, in the weak relativistic regime ($v \lesssim 50$), the fourfold RI cross section decreases $\sim v^{-\lambda}$ with $5.3 \lesssim \lambda \lesssim 5.8$ and the doubly differential RI cross section behaves like $v^{-\lambda+1}$ due to the extra v introduced by the scaling (3.8). This is slightly stronger than the first-order Born result (v^{-4} , Miraglia and Garibotti 1985). Considered as a function of momentum, the fourfold RI cross section decreases $\sim (\gamma v)^{-\lambda}$ with λ nearly constant (dropping from 5.1 to 4.7 when v increases from 20 to 100). In the ultrarelativistic limit ($\gamma \rightarrow \infty$) the total RI cross section $\sigma \sim \gamma^{-1}$. This is inferred from the Eichler (1990) result for REC since continuity across the ionization threshold implies the same behaviour for REC and RI.

4. Conclusion

A relativistic formulation of the IA has been provided in order to describe radiative ionization by very fast and very heavy projectiles. While the relativistic kinematics is treated exactly, the projectile scattering eigenstates are approximated by semirelativistic Sommerfeld–Maue wavefunctions. It was shown numerically that the RI differential cross section obtained in this way coincides with the nonrelativistic RI theory in the limit $\gamma \rightarrow 1$ and $Z_P \rightarrow 0$.

It has been found that, for fixed energy and forward emission of the electron, the features of the relativistic REC photon distribution are recovered for electron energies beyond the cusp energy: the angular distribution is not symmetric with respect to $\theta = 90^\circ$, but the peak is shifted to larger angles ($\theta_{peak} \sim 105^\circ$ for 400 MeV amu $^{-1}$ U $^{92+}$ + H, for all $E_f > \gamma c^2$). However when the energy is below the cusp, the θ distribution is skewed to smaller angles. The spectrum of the emitted photons is governed by the Compton profile of the initial state. This similarity of the photon features of RI and REC is due to the continuity across the ionization threshold.

If, on the other hand, the photon degrees of freedom are kept fixed (or integrated over), the electron spectrum for forward electron emission shows a double structure: on a background, which again is shaped by the target Compton profile, is superimposed the cusp-like peak as known from electron capture to continuum investigations. The shape of this cusp differs strongly, however, from the ECC cusp in that it sits on a Compton-profile-shaped background and has a considerably stronger asymmetry with a greater intensity on the high-energy side of the cusp. This difference is related to the fact that small momentum transfers govern the RI process whereas ECC requires the high momentum components of the initial bound state. The cusp asymmetry scales approximately with $Z_P/\gamma v$ for weakly relativistic systems but depends additionally on the photon emission direction in the general relativistic case.

We are confident that the approximations introduced to make the calculations feasible are well justified and do not affect our basic conclusions. Whenever $Z_P \gg Z_T$ and $\frac{1}{2}v^2 \gg |E_i^T|$, it is safe to neglect the binding energy compared to the electron's kinetic energy in the projectile frame of reference (the on-shell approximation), as well as the correlation energy in a multi-electron target (the single-particle approximation). This also allows for the omission of the electron–target interaction in the intermediate and final states (the IA), in particular since we deal with electron capture to continuum where the relative velocity between electron and projectile approaches zero.

Concerning the use of the Sommerfeld–Maue wavefunctions for the ejected electron, this is certainly a good approximation in the weak relativistic case (e.g. for 20 MeV amu Kr $^{36+}$ + H with $\gamma = 1.02$). Thus the strong asymmetry of the RI cusp is not altered by the use of these functions. For higher energies, if one trusts the IA, one can rely on previous investigations on the accuracy of the Sommerfeld–Maue wavefunctions within the bremsstrahlung calculations, since the folding with the initial-state momentum distribution

will not influence the applicability of these functions. Even for projectiles with high nuclear charge, Sommerfeld–Maue wavefunctions are expected to give reliable results since, in the case of RI, no high-momentum tails are involved because the emitted photon carries away all excess energy. This is in contrast to, for example, (e , $2e$) investigations where high momentum transfers are often required, making semirelativistic wavefunctions inappropriate.

Acknowledgments

I would like to thank S Hagmann for stimulating this work and for many fruitful discussions, and P A Amundsen for an important hint. I also want to express my gratitude to D Vernhet, H Rothard and CIRIL (France) for supporting contacts with the physical community.

References

- Anholt R *et al* 1984 *Phys. Rev. Lett.* **53** 234
 Bjorken D and Drell S D 1964 *Relativistic Quantum Mechanics* (Mannheim: BI)
 Briggs J S and Dettmann K 1974 *Phys. Rev. Lett.* **33** 1123
 Davidović D M, Moiseiwitsch B L and Norrington P H 1978 *J. Phys. B: At. Mol. Phys.* **11** 847
 Eichler J 1990 *Phys. Rep.* **193** 165
 Elwert G and Haug E 1969 *Phys. Rev.* **183** 90
 Geisenhofer E and Nakel W 1996 *Z. Phys. D* **37** 123
 Gould H, Greiner D, Lindstrom P, Symons T J M and Crawford H 1984 *Phys. Rev. Lett.* **52** 180
 Groeneveld K O, Meckbach W and Sellin I A (ed) 1984 *Forward Electron Ejection in Ion–Atom Collisions (Lecture Notes in Physics vol 213)* (Berlin: Springer)
 Hagmann S 2003 private communication
 Hino K and Watanabe T 1987 *Phys. Rev. A* **36** 581
 Ichihara A, Shirai T and Eichler J 1994 *Phys. Rev. A* **49** 1875
 Jakubaša-Amundsen D H 1983 *J. Phys. B: At. Mol. Phys.* **16** 1767
 Jakubaša-Amundsen D H 1997 *J. Phys. B: At. Mol. Opt. Phys.* **30** 365
 Jakubaša-Amundsen D H and Amundsen P A 1980 *Z. Phys. A* **297** 203
 Jakubaša D H and Kleber M 1975 *Z. Phys. A* **273** 29
 Kienle P, Kleber M, Povh B, Diamond R M, Stephens F S, Grosse E, Maier M R and Proetel D 1973 *Phys. Rev. Lett.* **31** 1099
 Kleber M and Jakubaša D H 1975 *Nucl. Phys. A* **252** 152
 Ludziejewski T *et al* 1998 *J. Phys. B: At. Mol. Opt. Phys.* **31** 2601
 Martiarena M L and Garibotti C R 1985 *Phys. Lett. A* **113** 307
 Moshhammer R *et al* 1994 *Phys. Rev. Lett.* **73** 3371
 Nordsieck A 1954 *Phys. Rev.* **93** 785
 Raisbeck G and Yiou F 1971 *Phys. Rev. A* **4** 1858
 Rose E M 1971 *Relativistic Electron Theory* vol 1 (Mannheim: BI) section III
 Schnopper H W, Betz H-D, Delvaile J P, Kalata K, Sohval A R, Jones K W and Wegner H E 1972 *Phys. Rev. Lett.* **29** 898
 Shaffer C D, Tong X-M and Pratt R H 1996 *Phys. Rev. A* **53** 4158
 Spindler E, Betz H-D and Bell F 1979 *Phys. Rev. Lett.* **42** 832
 Stöhlker Th, Mokler P H, Kozhuharov C and Warczak A 1997 *Comments At. Mol. Phys.* **33** 271
 Stöhlker Th *et al* 1995 *Phys. Rev. A* **51** 2098
 Stöhlker Th *et al* 1998 *Phys. Rev. A* **58** 2043
 Talman J D 1978 *J. Comput. Phys.* **29** 35
 Tseng H K and Pratt R H 1971 *Phys. Rev. A* **3** 100
 Yamadera A, Ishii K, Sera K, Sebata M and Morita S 1981 *Phys. Rev. A* **23** 24

[See endnote 2](#)

Queries for IOP paper 57703

Journal: **JPhysB**

Author: **D H Jakubaša-Amundsen**

Short title: **Radiative electron capture to continuum in relativistic ion–atom collisions**

Page 17

Query 1:

Author: 'Miraglia and Garibotti 1985' not in reference list.

Page 19

Query 2:

Author: should 'Jakubaša D H' in refs 16 and 18 be changed to 'Jakubaša–Amundsen D H'? Please check